COMPUTATIONAL ANALYSIS OF SIZE EFFECTS IN CHIRAL UNIT CELLS FOR MANDIBULAR IMPLANTS

Anne Grietinus Feenstra

S4782135

Computational Mechanical and Materials Engineering Group (ENTEG)

Period: 14/04/2025- 01/09/2025

Bachelor's project

1st Examiner: Antonis Vakis

2nd Examiner: Anastasiia Kruschynska

Daily supervisor: H.C.V.M.S. Veluvali

Table of Contents

1. Abstract

To find solutions in preventing the occurrence of stress shielding with mandibular implants, Finite Element Analysis (FEA) of Ti-6Al-4V metamaterial geometries composed of chiral unit cells was conducted. The geometries are varying between chiral-, anti-chiral- and combined lattices of dimensions n x n x n (n x 2n x n for the combined lattices) within a fixed volume. All structures were subjected to pure compression, torsion and shear, showing size-effects through a decreasing rate of stiffening for lattices under pure compression with an increase in amount of unit cells, and a decreasing rate of softening for lattices under pure torsion and shear. The computed moduli were then normalized by dividing them by obtained homogenized moduli values, to see whether they resembled the homogenized material's behavior. Though the moduli are computed to be too low to match cortical bone, these trends could provide an insight in how the moduli develop as the number of unit cells increases and how modifying the geometry of chiral unit cells may result in a higher probability of reducing stress shielding and thus ultimately reducing the need for revisional surgery.

2. Introduction

Reconstructive jaw surgery may be necessary following trauma, disease-related bone damage, or purely for cosmetic reasons. If a larger section of the jaw needs to be replaced, mandibular reconstruction through a free vascularized bone flap (van Gemert, 2012) can be used, or a mandibular implant is surgically inserted and fixed in place to the intact parts of the lower jaw (mandible) and chin using screws, as can be seen below in *Figure 1*:

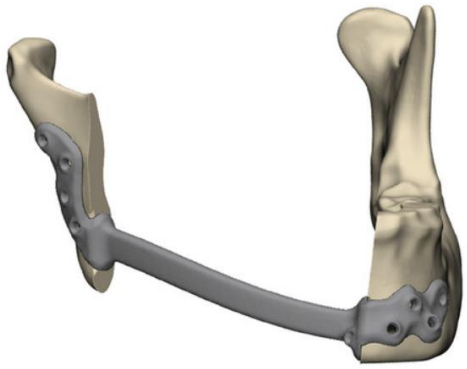

Figure 1: Solid titanium implant, fixed to the bone with screws. Reproduced from (Heins, 2025).

The most commonly used materials for mandibular implants include titanium or titanium alloys - for example Ti-6Al-4V – because of their good biocompatibility, durability and osseointegration promotion (Chung, 2016).

The solid titanium implant in this project will replaced by a metamaterial structure which enables to gain more control over design parameters by generating a periodic structure

composed of unit cells. The control over design parameters makes it so that these metamaterials can have well-defined mechanical properties, like Young's Modulus, shear modulus and poison's ratio. The geometry of these materials can be designed on micro-scale to regulate their mechanical response (Heins, 2025). With this tunability, it is possible to use metamaterials to close the gap between the Young's- and shear modulus of the titanium implant and cortical bone.

A well-designed mandible implant should be able to withstand chewing forces, which vary depending on implant size, patient anatomy and diet. Additionally, it should ensure a good distribution of loading stresses along the implant and surrounding bone. This is difficult, however: temporomandibular joint movement is not restricted to one plane and therefore it is hard to predict stress distribution under loading. Furthermore, the large mismatch in moduli between the jawbone and titanium (or titanium alloys) causes stress shielding, which in turn can cause a decrease in bone density (in accordance to Wolff's Law (Rowe, 2023)), aseptic loosening and ultimately implant failure. The failure of a mandibular implant often requires patients to undergo revision surgery, which is unnecessarily invasive and costly in terms of finance and time.

3. Literature review

3.1 Metamaterials

Rather than using conventional materials for replacement of the prosthetic, metamaterials were chosen for this particular project. These metamaterials are repeating structures that are composed of unit cells, the smallest repeating section of the metamaterial. These unit cells govern the behavior of the metamaterial. Metamaterial structures are tunable in their mechanical properties and can take periodic structures of different kinds of unit cells, each eliciting unique, often unusual behavior, such as negative Poisson's ratio (NPR) (Suhas P., 2025) . In contrast to foams that are also used in implant technology, metamaterials provide control over design parameters and are more reliable in terms of prediction of mechanical properties. There are, however, novel methods proposed that enable production of foams with controllable volume fractions and porosity (Yaqoob, 2023).

The material in this research is also porous and comprised of a repetitive structure called a unit cell. The unit cell can in turn be designed and finetuned to elicit certain unique, unusual mechanical properties that could improve the functionality of a prosthetic. With the right modifications, metamaterials could be used to mimic the mechanical properties of human bone, which could greatly improve implant functionality and prevent stress shielding. For this study in particular, the concept of chiral unit cells is introduced to replace the solid titanium parts of the mandibular implant at the connection sites with the jawbone and chin.

3.2 Chirality

As mentioned, a repetitive structure of chiral unit cells forms the metamaterial in this project. These lightweight three-dimensional structures with equal sides along all planes have a geometry that is asymmetric and will not give the same image when superimposed upon its mirror image (Fecher, 2022). Chiral unit cells can have very different geometries, with several shown in *Figure 2*.

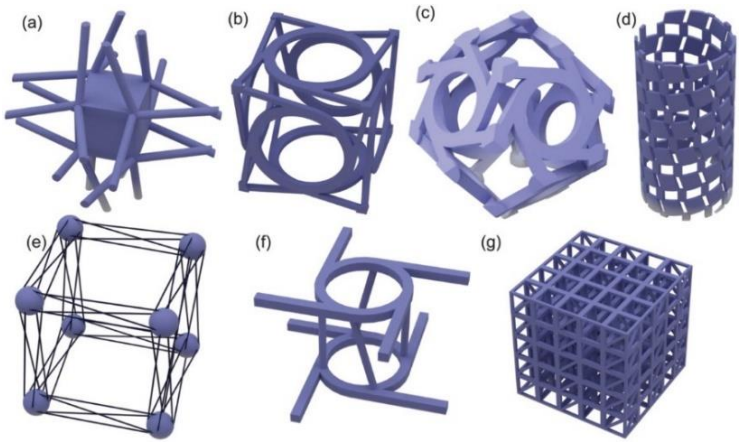

Figure 2: different 3D chiral unit cells. Reproduced from (Fernandez-Corbaton I., 2019)

Chirality in a material gives rise to a very unique mechanical property called tension-torsion coupling (TTC): When tensile or compressional forces are applied to a chiral structure, it induces twisting deformation and vice versa (Zheng, 2019). If a lattice is made of repeating chiral unit cells, compression will induce a twist within the structure with a certain twist angle. The basic unit cell used in the computational analysis for this study is similar to the illustration shown in *Figure 3*, with radii r_1 and r_2, ligament width t, thickness h and wall length l.

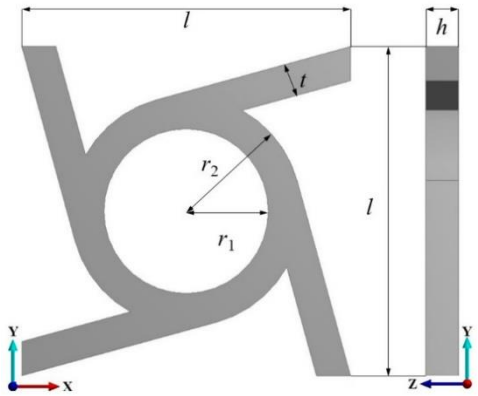

Figure 3: a plane projection of chiral unit cell. Reproduced from (Akhmetshin, 2023)

When an anti-chiral unit cell (i.e., the mirror image of the original unit cell) is introduced in a lattice in equal ratios chiral and anti-chiral, a structure can be developed with ideally net-zero rotation when compression is applied. This is because the rotation of the chiral section of the lattice is more or less “cancelled out” by the rotation of the anti-chiral section. Since we are looking at very small deformations, this is however not substantial to this research. The unit cells are depicted in *Figure 4*:

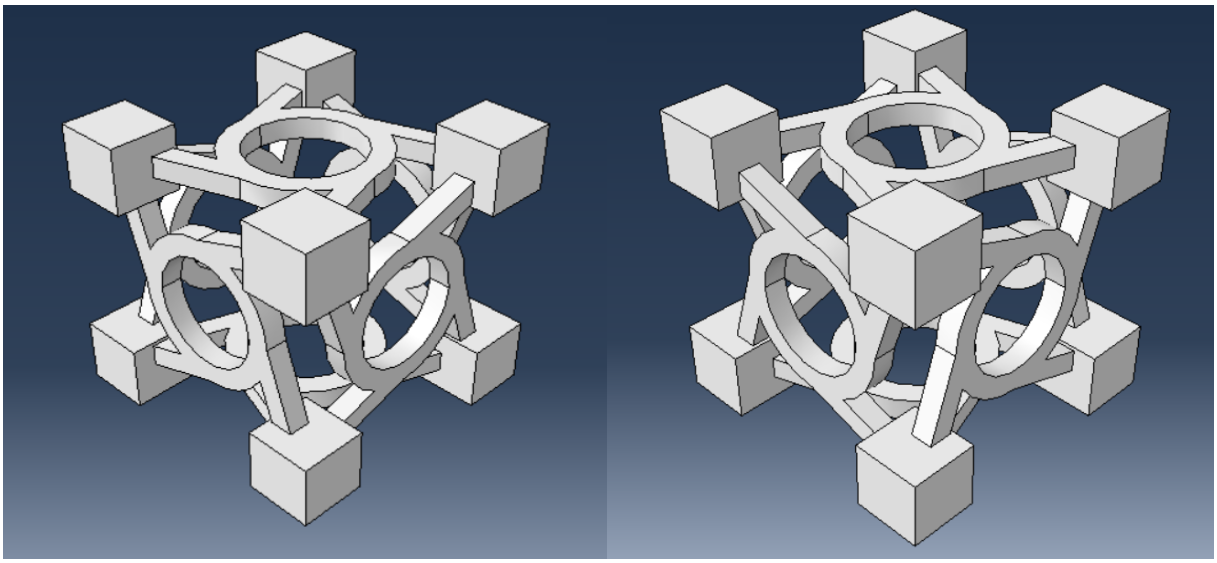

Figure 4: The used chiral (L) and anti-chiral (R) unit cells.

3.3 Stress-shielding

A mandibular implant gives rise to mechanical loading situations that do not occur under natural circumstances. When a patient receives a mandibular implant, the stresses induced by tasks the jaw performs are supposed to be distributed along the jawbone, but are for a part absorbed by the implant. Although there is a lack of worldwide consensus on modulus values and varying patient specificity for a value of Young’s modulus for cortical bone, with different setups yielding different measurements, varying between 5.466 and 17 GPa (Merema B. B., 2020). (Morgan, 2018) states that the shear modulus of cortical (femoral) bone is between 3.3 and 6 GPa. Nevertheless, it quickly becomes apparent that any of these values does not come close to the moduli of Ti-6Al-4V, which are around $E = 110\ GPa$ and $G = 44\ GPa$.

Because of this large mismatch in Elastic moduli, the bone is “shielded” from incoming loading stresses by the implant and becomes underloaded. In the long term, stress shielding will lead to resorption of the insufficiently loaded areas of bone around the implant, which in turn can cause implant loosening (Goharian, 2022). Eventually, this causes discomfort and pain to the patient and may require them to have revision surgery. Since this can all be regarded as unnecessarily invasive and costly, a solution to prevent stress-shielding is needed where the gap between Young’s moduli is reduced to more resemble original bone structure, to then promote osseointegration and proper functioning of the implant.

3.4 Size-effects

The mechanical behavior of a material can change depending on its physical dimensions. While mass and volume remain the same but size increases or decreases, the mechanical properties change. This phenomenon is known as a size-effect. The properties that change include - but are not limited to - the Young's modulus and shear modulus. For linear elastic deformations in metamaterials in particular, the size-effects have not been explored as much as they have been for conventional geometries. If these size-effects within a periodic metamaterial structure are known, they can be used in manufacturing to adjust a structure to ensure it yields the desired mechanical properties and to prevent prosthetic dysfunctionalities.

Since for this research the magnitude of deformations will be within the linear elastic region of the material, it is possible look at the material responses and size-effects that may occur under pure compression, pure torsion and pure shear separately.

4. Problem analysis

With the higher goal of reducing stress shielding in mandibular implants in mind, the aim of this research is to quantify size effects in metamaterial structures comprised of chiral unit cells to improve long-term functionality of the prosthesis, reduce the risk of bone resorption and implant loosening, and thus minimize need for revisional surgery.

While different variations of a metamaterial could possibly suffice, a chiral unit cell is chosen specifically as the building block for this project to see how its mechanical properties (E, G, ν) compare to those of cortical bone. Through computational analysis conducted in ABAQUS, this research will explore how varying size of the chiral, anti-chiral (n x n x n unit cells) and combined lattices (n x 2n x n unit cells) within a predefined space (1 x 1 x 1) could impact the implant's performance by investigating the changes of Young's modulus, Shear modulus under torsion and shear modulus under shear for different numbers of unit cells. In general, an increase in in moduli would mean a stiffer response when subjected to its associated type of deformation.

As these trends in change of moduli are made visible, this information can be used to determine how a metamaterial mandibular implant could be designed in order to decrease the mismatch between the moduli of cortical bone and the Ti-6Al-4V implant.

5. Methods and tools

The computational analysis for this research was conducted in the Finite Element Modeling (FEM) software called ABAQUS. Since this program requires a large amount of processing power and physical memory, it was conducted on a high-performance PC (16GB RAM and an Intel Core i7-12700 processor).

In order for the simulations to run properly and emulate the real-life situation as accurately as possible, the geometry, material properties, mesh size, constraints and boundary conditions need to be well-defined. For pure compression, torsion and shear, the material properties and way of assembling the geometry are all roughly the same. The boundary conditions are differently defined for all types of deformation and are clarified in more detail in this section. Additionally, the right mesh sizes need to be determined and since the key interest is in the behavior of the chiral and anti-chiral unit cells, we also need to include loading of the plates in the final configurations. The trends in change for normalized Young's modulus under pure compression (E/E^*), shear modulus under pure torsion (G_Γ/G_Γ^*) and pure shear (G_τ/G_τ^*) will be investigated. How the values for E, G_Γ and G_τ and their homogenized counterparts (E^*, G_Γ^* and G_τ^*) were calculated is also discussed in this chapter.

5.1 Geometry

The elemental building block for this project is the chiral unit cell, in structures fixed between plates of equal thickness (h = 0.05) to ensure uniform load distributions across the surface. For the sake of simplicity, the dimensions of the unit cell are 1mm x 1mm x 1mm. When running simulations of geometries with higher order lattices up to 5 x 5 x 5, these same dimensions will be used: the unit cells will be scaled down to fit within the original 1 x 1 x 1 dimensions. For example, when looking at the 2 x 2 x 2 lattice, it is comprised of 8 unit cells, each having 0.5 times their original dimensions (0.5mm x 0.5mm x 0.5mm). To visualize this process, creating the assemblies for the 2 x 2 x 2 and 5 x 5 x 5 lattices will look as shown in *Figure 5*. The assemblies consisting of only anti-chiral unit cells look similar, only mirrored.

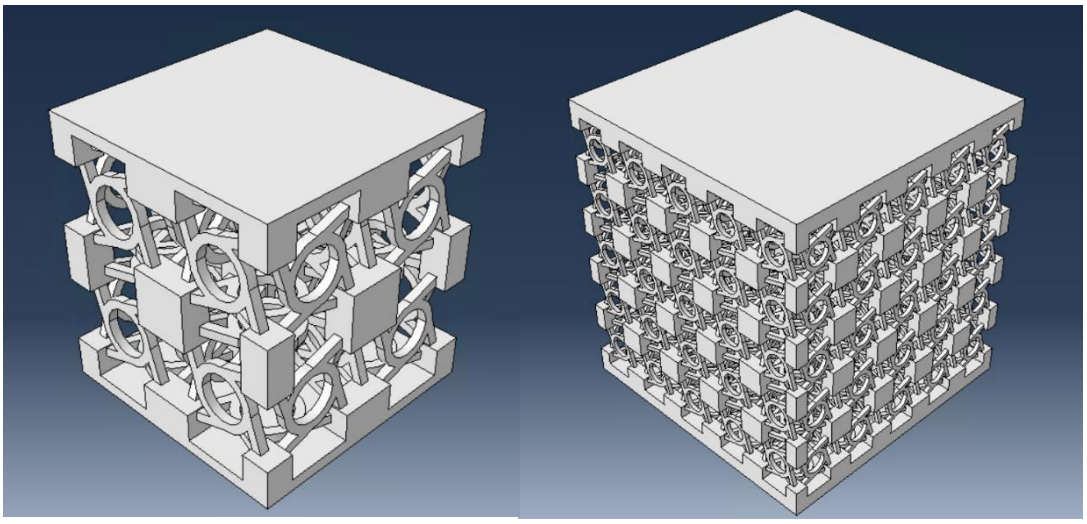

Figure 5: 2 x 2 x 2 and 5 x 5 x 5 Chiral Lattices.

The size effects in these structures is compared to the combined lattices, which are formed by the chiral structure stacked upon the anti-chiral structure, meaning it is the entire chiral geometry connected to the entire anti-chiral structure.

Combining the assemblies of chiral and anti-chiral lattices gives structures for the 2 x 2 x 2 and 5 x 5 x 5 lattices as shown in *Figure 6*. Note that despite the combined structures are technically twice as large in height, they were still named in the same fashion as the chiral and anti-chiral structures in the results, for the sake of consistency. The influence of the height difference is however not neglected in the calculations.

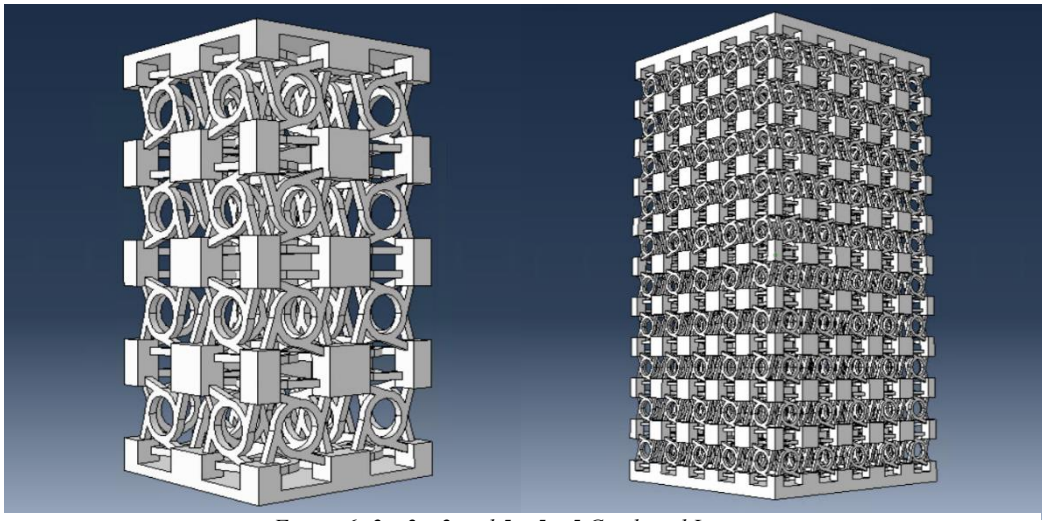

Figure 6: 2 x 2 x 2 and 5 x 5 x 5 Combined Lattices.

5.2 Material definition

As aforementioned, Ti-6Al-4V is a material commonly used in biomedical engineering and implant technology. For that reason, it is chosen as the material for computational analysis. The Young's modulus and Poisson's ratio of Ti-6Al-4V (Merema B. B., 2020), were defined in ABAQUS as $E = 110\ GPa$ and $\nu = 0.343$ respectively.

5.3 Constraints

Defining the constraints for the simulations is important because they define the relationship between the motion different regions of the geometry. For all types of deformations, rigid body constraints were created for the top and bottom surfaces of the lattices to ensure the relative distances between nodes within the constraint remain the same during deformation. In addition, they were related to reference points (RP1 and RP2) located in the middle of these surfaces How these constraints were defined is shown in *Figures 7 and 8:*

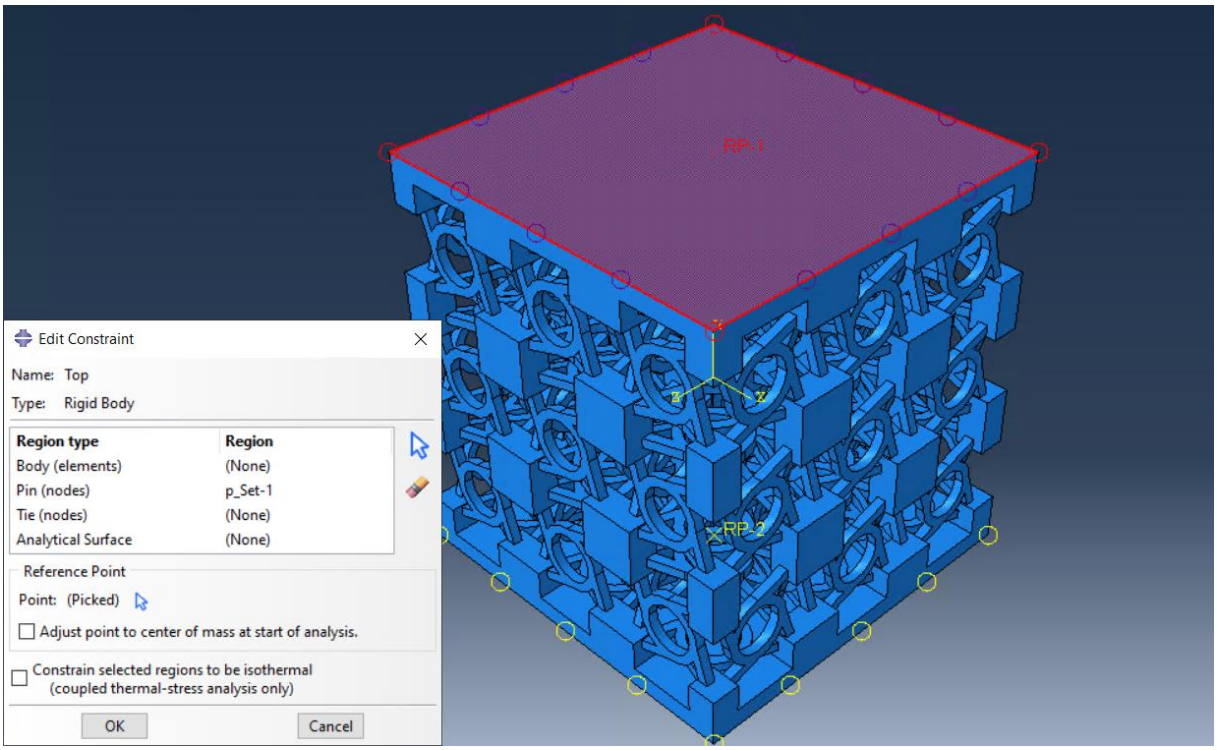

Figure 7: Constraint for top section of the lattice.

For the constraint of the bottom section:

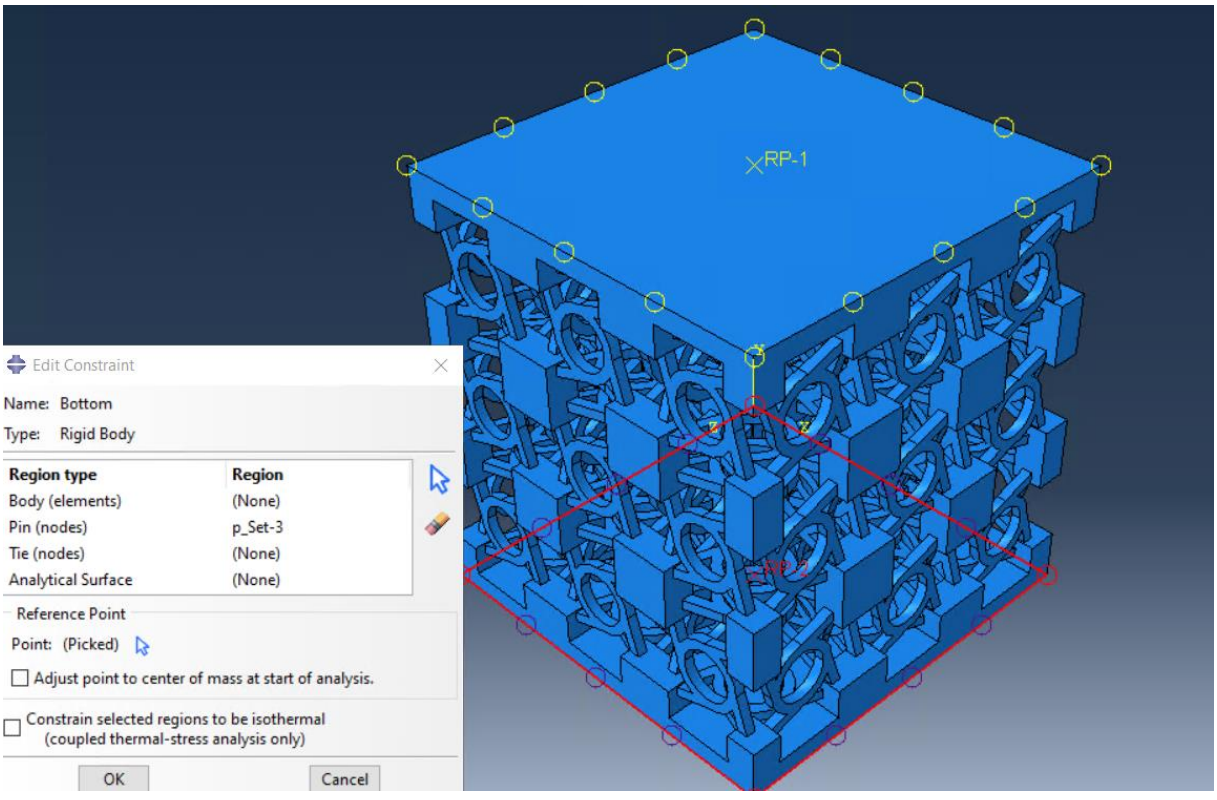

Figure 8: Constraint for bottom section of the lattice.

For pure shear models, the constraints are relatively more difficult as a third constraint needs to be added. This tie constraint consists of a master and slave surface that ensures they share the same motion. The main surface is chosen to be the surface towards which the shearing deformation is applied and thus the secondary surface will be on the opposite side of the structure. The tie constraint is restricted to allow a maximum distance of 1.1mm between these two surfaces, which is the total width of the structure with an offset of 0.1mm. How this constraint is defined is shown in *Figure 9:*

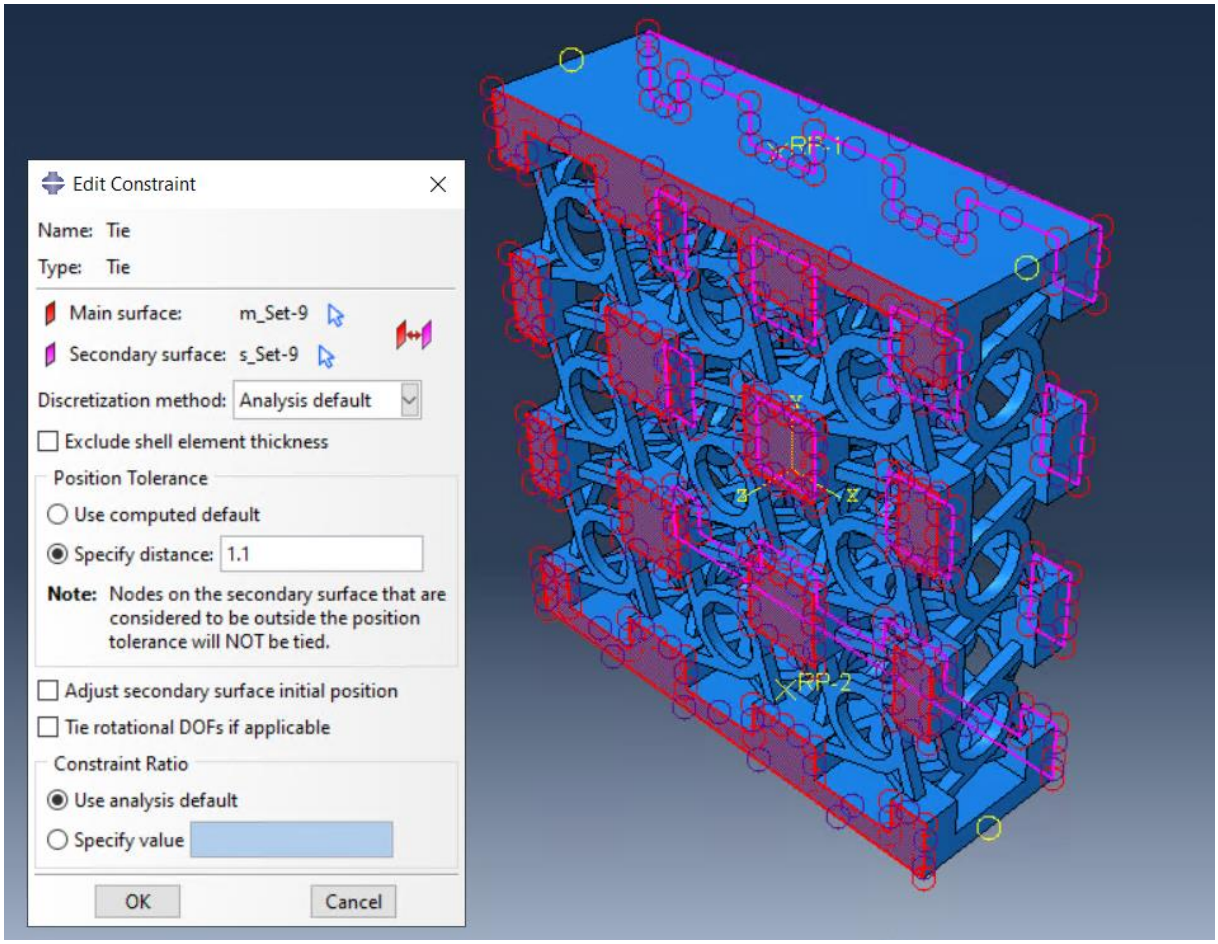

Figure 9: Tie constraint for shear models.

5.4 Boundary conditions

The boundary conditions that can vary for an assembly in ABAQUS are U1, U2 and U3, which stand for displacements in the x-, y- and z directions and UR1, UR2 and UR3, which stand for rotations along the x-, y- and z axes.

Firstly, for pure compression, the motion of interest is the compression in the vertical direction. To generate this motion in the model, the top section of the geometry was limited to only move in the y-direction. The bottom plate has fixed DOFs across the horizontal and vertical axes. Here, the x- and z- direction are horizontal whereas y-direction is vertical Rotational motion is not permitted.

For pure torsion, similar boundary conditions were applied. However, instead of vertical movement about the y-axis, the motion of interest is the rotation about the y-axis. In ABAQUS, this would mean changing U2 = 0.01 to UR2 = 0.01, inducing rotational displacement rather than vertical displacement On the bottom section of the geometry, a limited DOF for rotation about the y-axis (UR2) is added in combination with the limit across x-, y- and z- directions.

Lastly, for pure shear, the shearing motion was directed in the z-direction with movement in x- and y- direction set to zero. On the bottom section, the values of U1, U2 and U3 were all set to zero.

An overview of the loading types and boundary condition inputs for each loading type are described in *Table 1*. Any missing value of U1, U2, U3, UR1, UR2 or UR3 implies that they were not defined, meaning that particular DOF is free.

Loading type	**Boundary condition(s) top section**	**Boundary conditions(s) bottom section**
Compression	U2: -0.01	U1= U2= U3 = 0
Torsion	UR2: 0.01	U1 = U2 = U3 = UR2 = 0
Shear	U1 = U2 = 0 U3 = 0.01	U1 = U2 = U3 = 0

Table 1: Boundary Conditions in ABAQUS for each loading type.

5.5 Calculating the Young's modulus / Shear modulus

5.5.1 Compression

For the geometries loaded under pure compression, the Young's modulus is calculated by:

$$E = \frac{RF_2}{A\varepsilon} \tag{1}$$

Where RF_2 is the reaction force about the axis of compression (y-axis), divided by the surface area (A=1) multiplied by the strain (ε), which in turn is calculated by:

$$\varepsilon = \frac{u}{(l + 0.1)} \tag{2}$$

Note that here u = 0.01 and the 0.1 added to the length of the structure accounts for the total plate thickness.

5.5.2 Torsion

For the geometries loaded under pure torsion, the shear modulus (G_Γ) is calculated using the following formula:

$$G_\Gamma = \frac{M_z La}{J_T \theta_z} \tag{3}$$

Where M_z denotes the net reaction moment about the torsion axis, La the length of the structure along the torsion axis (=1.1 for only chiral or anti-chiral structures and 2.1 for the combined structures) and the angle of twist, θ_z, which for this research is defined as 0.01 rad. Lastly, J_t, the torsional constant of a rectangular base section, which is calculated by:

$$J_T = \frac{1}{16} w h^3 \left(\frac{16}{3} - 3.36 \frac{h}{w} (1 - \frac{h^4}{12 w^4}) \right) \quad (w \geq h) \tag{4}$$

With lengths of the sides w and h. However, since the lengths of our sides are both equal to 1, we can write this formula as:

$$J_T = \frac{1}{16} \left(\frac{16}{3} - 3.36 \left(1 - \frac{1}{12} \right) \right) \ (\cong 0.1408)$$

5.5.3 Shear

Under shear, the whole structure is expected to show shearing in a parallel relative to bottom surface, meaning the structure moves sideways in a parallel fashion while the bottom is fixed. That is why only using one column is representative for the shearing motion of the entire structure. Since only 1 column of the lattice is used for the shearing simulations, the plate surface area varies per lattice size.

The areas for each lattice size are computed according to *Table 2*:

Lattice size (nxnx1)	Plate surface area (A)
1	1 x 1
2	1 x 0.5
3	1 x 0.33
4	1 x 0.25
5	1 x 0.2

Table 2: Dimensions for plate surfaces of structures used for shearing simulations.

This is beneficial, because rendering and computing times are lowered. However, all modulus values should reference the same surface area as if it were still the original 1 x 1 x 1 dimensions (or 1x2x1 lattice for combined structures).

The measured shear modulus ($G_{\tau,}$) under pure shear is computed in a similar fashion to the Young's modulus in equation (1) and is calculated by the formula:

$$G_\tau = \frac{RF_3}{\varepsilon} \tag{5}$$

Where RF_3 is the reaction force about the z-axis (direction of shearing motion) divided by the reference surface area from the original 1x1 plate (A_{ref}) multiplied by the strain (ε). To make it resembles the total lattice structure, equation (5) is used to calculate the scaled shear modulus ($G_{\tau,norm}$) by multiplying it by the plate surface area:

$$G_{\tau.scaled} = G_\tau * A \tag{6}$$

5.6 Mesh convergence analysis

To ensure accurate results from the ABAQUS simulations, it is important to determine a mesh size that is sufficiently fine enough to provide the most accurate results relative to the lowest computation time. The mesh type that was chosen for the study use tetrahedral elements (C3D10). At a certain point there should be an optimum, where refining the mesh size more will only yield higher computation times while the calculated results stay within an acceptable margin of deviation. This relative error (RE) is determined by computing the deviation of the reaction force value compared to the reaction force corresponding with the finest mesh size that was taken (0.0125 in this case). If this relative error has a margin around or lower than 1%, it is deemed acceptable and the mesh size can be used for further simulations.

The relative error was calculated using:

$$RE = \frac{E_{mesh} - E_{finest\ mesh}}{E_{finest\ mesh}} * 100\% \quad \text{or} \quad RE = \frac{G_{mesh} - G_{finest\ mesh}}{G_{finest\ mesh}} * 100\% \tag{7}$$

When a valid element size is known, the number of elements for one unit cell should be known as well. With that knowledge, it should be possible to determine how to scale the mesh size with increase in unit cells.

5.6.1 Mesh convergence – Compression

For Chiral / Anti-chiral structures:

Approximate global seed size	Number of elements	Young's modulus (Pa)	Relative error (%)
0.1	2836	1.307E+09	32.2
0.05	18926	1.049E+09	6.01
0.025	122451	1.007E+09	1.82
0.020	263412	1.001E+09	1.13
0.015	555009	9.929E+08	0.36
0.0125	945363	9.893E+08	0

Table 3: Mesh convergence analysis for Chiral and Anti-chiral structures under pure compression

For Combined structures:

Approximate global seed size	Number of elements	Young's modulus (Pa)	Relative error (%)
0.1	4521	1.152E+09	24.5
0.05	31708	9.883E+08	6.73
0.025	200339	9.443E+08	1.99
0.020	432322	9.361E+08	1.10
0.015	901887	9.290E+08	0.33
0.0125	1546449	9.259E+08	0

Table 4: Mesh convergence analysis of combined structures under pure compression

This gives the following figures for the relative errors:

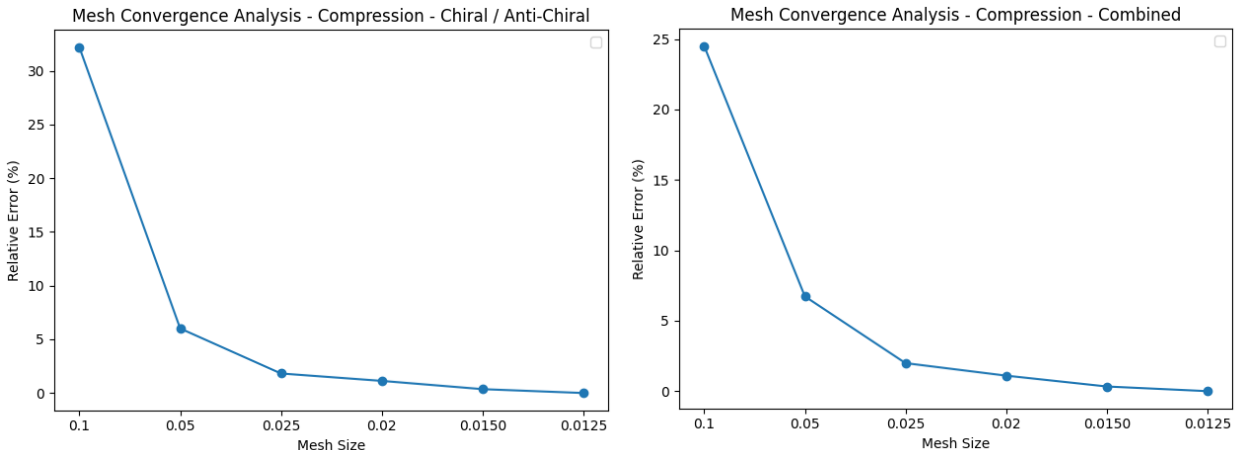

Figure 10: Relative error versus mesh size - pure compression

For both types of structures, there is a small difference between the relative errors of mesh sizes 0.020 and 0.015. For the sake of keeping the computing times and physical memory usage reasonable, mesh size 0.02 is deemed acceptable for compression models of a 1 x 1 x 1 structure.

5.6.2 Mesh convergence – Torsion

For Chiral / Anti-chiral structures:

Approximate global seed size	Number of elements	Shear Modulus (Pa)	Relative error (%)
0.1	2836	6.111E+08	11.4
0.05	18926	5.637E+08	2.78
0.025	122451	5.526E+08	0.75
0.020	263412	5.507E+08	0.40
0.015	555009	5.492E+08	0.13
0.0125	945363	5.485E+08	0

Table 5: Mesh convergence analysis for Chiral and Anti-chiral structures under pure torsion

For Combined structures:

Approximate global seed size	Number of elements	Shear Modulus (Pa)	Relative error (%)
0.1	4521	5.293E+08	11.9
0.05	31708	4.871E+08	2.93
0.025	200339	4.768E+08	0.77
0.020	432322	4.751E+08	0.41
0.015	901887	4.738E+08	0.12
0.0125	1546449	4.732E+08	0

Table 6: Mesh convergence analysis for combined structures under pure torsion

This gives the following figures for the relative errors:

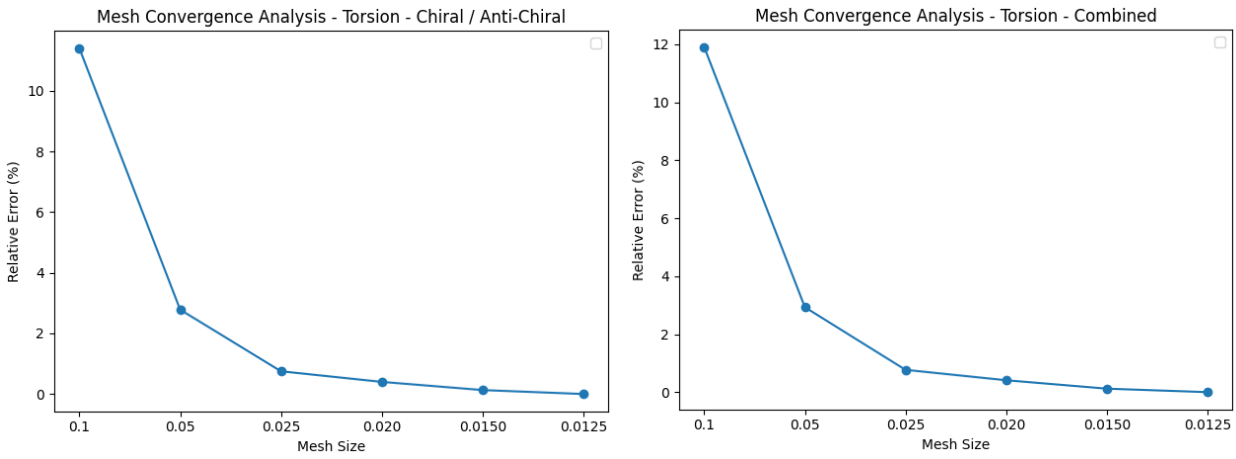

Figure 11: Relative error versus mesh size - pure torsion

The global seed size of 0.025 is deemed acceptable for Chiral and Anti-chiral structures as well as the combined structures because it maintains a relative error lower than 1%, which is sufficient for the torsion simulations.

5.6.3 Mesh convergence – Shear

For Chiral / Anti-Chiral structures:

Approximate global seed size	Number of elements	Shear Modulus (Pa)	Relative error (%)
0.1	2836	3.504E+08	10.5
0.05	18926	3.252E+08	2.56
0.020	263412	3.193E+08	0.70
0.025	122451	3.182E+08	0.37
0.015	555009	3.174E+08	0.12
0.0125	945363	3.171E+08	0

Table 7: Mesh convergence analysis for Chiral and Anti-chiral structures under pure shear

For Combined structures:

Approximate global seed size	Number of elements	Shear Modulus (Pa)	Relative error (%)
0.1	4521	3.271E+08	10.4
0.05	31708	3.041E+08	2.60
0.025	200339	2.983E+08	0.66
0.020	432322	2.975E+08	0.37
0.015	901887	2.967E+08	0.11
0.0125	1546449	2.964E+08	0

Table 8: Mesh convergence analysis for combined structures under pure shear

This gives the following figures for at the relative errors:

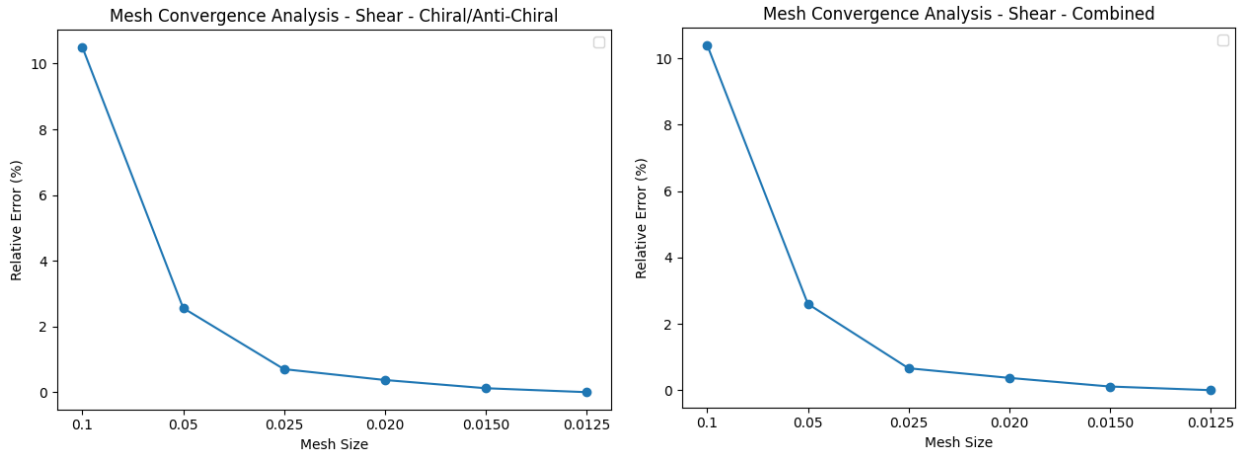

Figure 12: Relative error versus mesh size - pure shear

The global seed size of 0.025 is deemed acceptable for Chiral and Anti-chiral structures as well as the combined structures because it maintains a relative error lower than 1%, which means it is sufficient for the shear simulations.

Now the adopted mesh sizes can be scaled to be used in the lattices that contain more unit cells. This means that if we consider the largest lattices (5 x 5 x 5), we need to scale the mesh size down to 0.20 times its original value, as the length of the unit cell was decreased by a factor 0.20 to fit within the original dimensions. This means from the 3 x 3 x 3 lattice and onward, this results in extremely fine meshes. These cannot be ran on the computer used for this research. For this reason, the mesh sizes for the simulations were chosen as in *Table 9*:

Lattice type	**Deformation**	**Mesh sizes**
Chiral / Anti- Chiral	Pure Compression	For 1 x 1 x 1-2 x 2 x 2: 0.02 For 3 x 3 x 3 – 5 x 5 x 5: 0.01
Combined	Pure Compression	For 1 x 1 x 1-2 x 2 x 2: 0.02 For 3 x 3 x 3 – 5 x 5 x 5: 0.01
Chiral / Anti – Chiral	Pure Torsion	For 1 x 1 x 1-2 x 2 x 2: 0.025 For 3 x 3 x 3-4 x 4 x 4: 0.0125 For 5 x 5 x 5: 0.01
Combined	Pure Torsion	For 1 x 1 x 1-2 x 2 x 2: 0.025 For 3 x 3 x 3: 0.0125 For 4 x 4 x 4: 0.01 For 5 x 5 x 5: 0.0099
Chiral / Anti – Chiral	Pure Shear	For 1 x 1 x 1-2 x 2 x 2: 0.025 For 3 x 3 x 3 – 5 x 5 x 5: 0.0125
Combined	Pure Shear	For 1 x 1 x 1-2 x 2 x 2: 0.025 For 3 x 3 x 3-4 x 4 x 4: 0.0125 For 5 x 5 x 5: 0.01

Table 9: Chosen mesh sizes per deformation type and lattice size

5.7 Accounting for the plates

Since the chiral unit cells are fixed between two solid plates and the key interest is the size effects of the chiral unit cells, the plates in the models need to be accounted for to prevent influence of the final results. This was done by generating a separate model in ABAQUS, where a cube and rectangle with same dimensions as the normal and combine lattices were fixed between 0.05 thick plates. The cube and rectangle were given the same engineering constants for Young's modulus, shear modulus and Poisson's ratio as a homogenized chiral unit cell:

Property	**Cube**
E_1^*, E_2^*	1.525 GPa
E_3^*	0.363 GPa
G_{12}^*, G_{13}^*	0.363 GPa
G_{23}^*	0.363 GPa
ν_{32}^*, ν_{23}^*	0.0049
ν_{12}^*, ν_{21}^*	0.0049
ν_{21}^*, ν_{12}^*	0.0049

Table 10: Engineering constants of the cube and rectangle

They were then loaded under the same boundary conditions and constraints as the chiral structures. Running these simulations gave the following normalized moduli:

Lattice	**Homogenized moduli**
Normal (1x1x1)	$E^* = 1.676\ Gpa$ $G_\Gamma^* = 0.416\ Gpa$ $G_\tau^* = 0.399\ Gpa$
Combined (1x2x1)	$E^*_{combined} = 1.600\ Gpa$ $G^*_{\Gamma,\text{combined}} = 0.388\ Gpa$ $G^*_{\tau,combined} = 0.399\ Gpa$

Table 11: Homogenized moduli values for normal and combined lattices

When comparing the computed homogenized moduli to the engineering constants used, we can determine what influence the plating has on the overall structure. For $G^*_{\tau,combined}$, the same value as G_τ^* was used. When comparing the homogenized moduli, it becomes apparent that the homogenized moduli of the combined structures is slightly lower than those of normal structures of only chiral or anti-chiral cells. Additionally, when comparing the calculated homogenized moduli to the engineering constraints in *Table 10*, we see that the calculated values are slightly higher than the engineering constants: this overshoot is caused by the influences of the plates.

6. Results

The computed moduli were divided by the homogenized moduli obtained in section 5.7. The results for the Young's modulus and shear moduli of the lattices under pure compression, torsion and shear are shown in this section. Each subsection shows the plot for moduli of chiral, anti-chiral and combined lattices. These can be seen in *Figures 10-12*, combined with a stress field visualization of the 3 x 3 x 3 (and 3 x 3 x 1 for pure shear) lattices under their deformation modes. In the figures, $\frac{E}{E^*} = 1$ and $\frac{G}{G^*} = 1$ are highlighted, implying that values close to 1 should behave similarly to the homogenized material.

The following subsections will show the scatterplot for the normalized moduli for each deformation type for different numbers of unit cells.

6.1 Pure compression

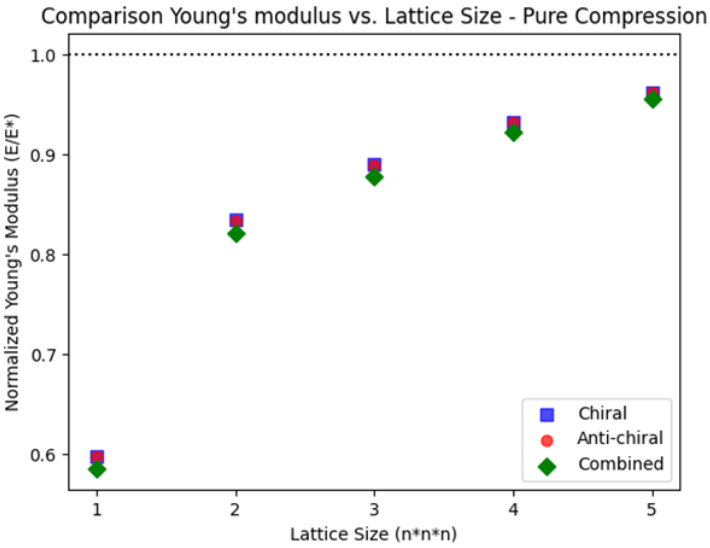

(a) (b)

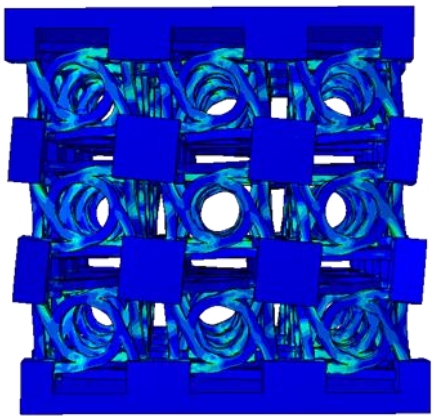

Figure 13: (a) Normalized Young's modulus versus lattice size - Pure compression, (b) stress field of 3x3x3 lattice under pure compression.

6.2 Pure torsion

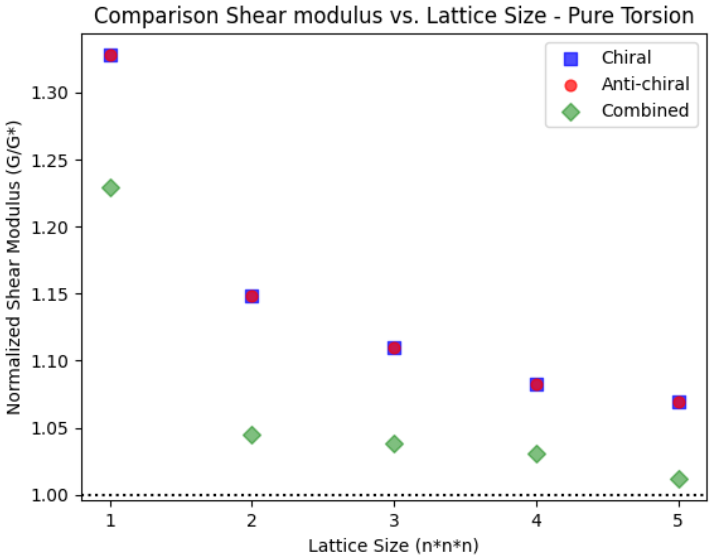

(a) (b)

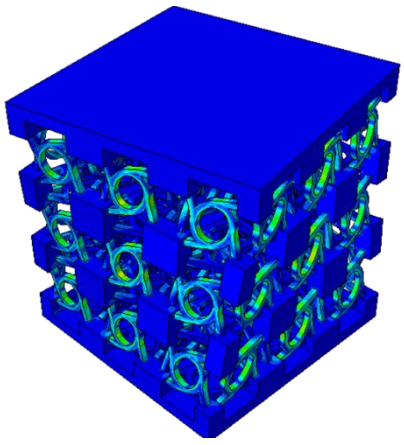

Figure 14: (a) Normalized Shear modulus versus lattice size - Pure torsion, (b) Stress field of 3x3x3 lattice under pure torsion

6.3 Pure Shear

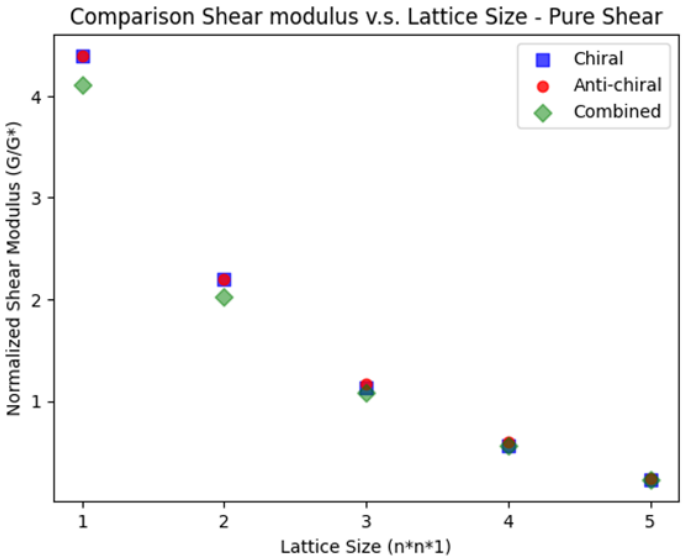

(a)

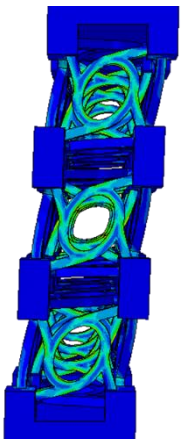

(b)

Figure 15: (a) Normalized Shear modulus versus lattice size – Pure shear, (b) Stress field of 3x3x3 lattice under pure shear

7. Discussion and conclusion

7.1 Discussion

7.1.1 Pure compression

Under pure compression, the structures show a higher Young's modulus with an increasing number of unit cells, which means it is stiffening as the number of unit cells increases. The increase in number of unit cells means the geometry gets denser with unit cells, making it behave stiffer. The rate of change also decreases as the number of unit cells increases, converging to 1. The normalized moduli converging to 1 implies that at higher counts of unit cells, the metamaterial resembles the behavior of the homogenized chiral unit cells. The values of E for chiral and anti-chiral lattices are roughly the same. The combined lattice show similar behavior, only with slightly lower Young's moduli, which can be explained by the increased height of the lattice. The highest absolute value Young's modulus measured belongs to the 5 x 5 x 5 anti-chiral lattice and is equal to $E = 1.612\ Gpa$, (Appendix A), which is still significantly lower than the Young's modulus of cortical bone. The unit cell (or a new unit cell) should be developed that shows a stiffer response to compression to be viable for use in the mandibular implant.

7.1.2 Pure torsion

Under pure torsion, the structures show a decreasing shear modulus with an increasing number of unit cells, meaning it is showing softening behavior. The rate of change also decreases while the number of unit cells increases. The values for chiral and anti-chiral lattices are roughly the same. The combined lattices show similar behavior only with a very flattening convergence, which is most likely caused by under-meshing. The mesh size of the final combined lattice was arbitrarily decreased to see if any finer mesh size would give a different result, but for any mesh size under 0.0099, the application ran out of physical memory. To circumvent this, the simulations could be run on a system that has more physical memory or perform homogenization on the model. The highest computed shear modulus under pure torsion is $G_\Gamma = 0.5525\ Gpa$ (Appendix A) and was computed based on the 1 x 1 x 1 chiral lattice. It is way lower than the shear modulus of cortical bone (3.3 – 6 GPa). It is therefore safe to say that based on this model, the shear modulus of this specific chiral unit cell design is too low to resemble that of cortical bone and therefore is not a viable replacement with its current shape and properties. It needs modifications to its structure so that it will elicit less softening behavior when loaded under torsion so that it can be used in mandibular implants.

7.1.3 Pure shear

Under pure shear, the structures show a lower shear modulus with an increasing number of unit cells, meaning it is also showing softening behavior for this type of deformation. What may be surprising is that here, all models elicit similar behavior despite the combined model having a larger height. It appears that the increase in height barely affects the values of shear modulus under pure shear. This could be related to the homogenized G_τ^* value, which was not possible to be calculated for the combined lattices due to unsolvable overconstraining issues within the ABAQUS model.

7.2 General Conclusion

In general, we can state that under pure compression, the increase in unit cells results in a stiffening response in chiral lattices and a softening response in lattices that under pure torsion and shear. It is shown that for pure compression and the combined model for torsion, the values of $\frac{E}{E^*}$ and $\frac{G_\Gamma}{G_\Gamma^*}$ converge to 1 whereas for the other models, they do not. When looking at the maximum computed values of the moduli for each deformation mode, they do not come anywhere near the mechanical properties of cortical bone. Although this means that in terms of moduli it does not resemble cortical bone, it does not render this metamaterial entirely useless: further optimization of the design needs to be done and how it behaves within a mandible needs to be analyzed before ruling out its viability. Research into modifications of

the chiral unit cell, such as adjusting the arm width and ring diameter is needed in order to find a unit cell with moduli more similar to cortical bone.

7.3 Limitations and further research

Although these plots could provide a valuable insight into how size effects develop in chiral metamaterials, more research is needed for developing a prosthetic that uses metamaterials and chiral unit cells in particular. Different modifications of the used chiral unit cell can be tested to check if the size effect trends still hold and to verify if these can produce higher Young's and shear moduli to become more mechanically similar to cortical bone. Additionally, other designs of metamaterials can be used in research comparable to this one, in order to see what size effects occur for different structures, like cubic, honeycomb or auxetic metamaterials.

8. Ethics

With the undeniable growth in influence of generative Artificial Intelligence (GenAI) on scientific research and society as a whole, the final part of this report is dedicated to discussing how GenAI was used during this project. In accordance with the rules of responsibly using GenAI as described in the "Ten UG Basic Rules for Use of AI in Teaching", Artificial Intelligence was used merely as a tool in supporting me in writing the project rather than letting it write it for me. In particular, I consulted ChatGPT to verify my formulation, grammar and spelling in the report writing. As users of generative AI might also know, is that ChatGPT often offers alternative writing solutions. I have elected to not use said alternative in applicable situations, in order to ensure there would be no submission of literal AI output. No suggestions provided by ChatGPT were used before consulting the internet to verify the given information. For personal reassurance, this paper was ran through several AI / plagiarism checkers, yielding a percentage of presumed AI-usage not higher than 1%.

I think it is safe to say this research is morally acceptable, since only 3D models on a computer were involved in conducting this research. To guarantee ethically responsible research in the future, all learning models using personal data (like medical records) should always be used in a responsible fashion and in consultance with the patients involved.

Lastly, on a more personal note, I definitely believe that Artificial Intelligence should be embraced in academia and used responsibly as a tool in accelerating progress and advancement in science. It has made its way into our lives, just like the internet and mobile phone before, and is certainly here to stay.

Relevant articles:

- Alfaraj, A. et al. (2024). *Race to the Moon or the Bottom? Applications, Performance and Ethical Considerations of Artificial Intelligence in Prosthodontics and Implant Dentistry.* Dentistry Journal, Volume 13. DOI: https://doi.org/10.3390/dj13010013
- Panahi, O, & Farrokh, S. (2025). *Ethical Considerations of AI in Implant Dentistry: A Clinical Perspective.* Jounral of Clinical Review & Case Reports, 10(2). DOI: https://www.researchgate.net/profile/Omid-Panahi/publication/389324381_Ethical_Considerations_of_AI_in_Implant_Dentistry_A_Clinical_Perspective/links/67beabef645ef274a494c7b0/Ethical-Considerations-of-AI-in-Implant-Dentistry-A-Clinical-Perspective.pdf
- Rokshad, R. et al. (2023). *Ethical considerations on artificial intelligence in dentistry: A framework and checklist*. Journal of Dentistry, Volume 135. DOI: https://doi.org/10.1016/j.jdent.2023.104593

Bibliography

- Akhmetshin, L. L. (2023). Influence of Topological Defects on the Mchanical Response of Unit Cells of the Tetrachiral Mechanical Metamaterial. *7*(129).
- Chung, D. (2016). *Carbon Composites (Second Edition) - Chapter 7 - Carbon-Matrix Composites.* Butterworth-Heinemann.
- Eskandari, S. S. (2024). Unravelling Size-Dependednt and Coupled Properties in Mechanical Metamaterials: A Couple-Stress Theory Perspective. *Advanced Science*.
- Fecher, G. H. (2022). Chirality in the Solid State: Chiral Crystal Structures in Chiral and Achiral Space Groups. *15*(17).
- Fernandez-Corbaton I., e. a. (2019). New Twists of 3D Chiral Metamaterials. *31*(26).
- Goharian, A. &. (2022). *Interactions of Bone with Orthopedic Implants and Possible Failures.* Elsevier.
- Heins, J. M. (2025). Mandibular Implants: A Metamaterial-Based Approach to Reducing Stress Shielding. *Advanced Healthcare Materials*.
- Liang, X. e. (2022). Active design of chiral cell structures that undergo complex deformation under uniaxial loads. *217*.
- Lynnerup, N. &. (2019). *Ortner's Identification of Pathological Conditions in Human Skeletal Remains (Third Edition) - Chapter 4 - Fundamentals of Human Bone and Dental Biology: Structure, Function and Development.* Academic Press.
- Merema, B. B. (2020). Novel finite-element based plate design for bridging mandibular defects: Reducing mechanical failure. *Oral Diseasess*, 1265-1274.
- Merema, B. B. (2020). Patient-specific finite element models of the human mandible: Lack of consensus on current set-ups. *Oral Diseases*, 42-51.
- Morgan, E. F. (2018). Bone Mechanical Properties in Healthy and Diseased States. *Annual Review of Biomedical Engineering*, 119-143.
- Rho, J. Y. (1933). Young's modulus of trabecular and cortical bone material: ultrasonic and microtensile measurements. *26*(2).
- Rowe, P. K. (2023). *Physiology, Bone Remodeling.* Retrieved from StatPearls.
- Suhas P., Q. J. (2025). A review on mechanical metamaterials and additive manufacturing techniques for biomedical applications. (3).
- van Gemert, J. T. (2012). Free Vascularized Flaps for Reconstruction of the Mandible: Complications, Success and Dental Rehabilitation. *Journal of Oral and Maxillofacial Surgery*, 1692-1698.
- Yaqoob, K. A. (2023). Novel Method for the Production of Titanium Foams to Reduce Stress Shielding in Implants. *ACS Omega*, 1876-1884.
- Zheng, B. e. (2019). A novel metamaterial with tension-torsion coupling effect. *171*.

Appendix

Appendix A: Google Colab-file used for data and data processing

Link to the drive-file:
https://colab.research.google.com/drive/16hqSeKGOBg9wzBjpewq9NjtwUXiiXkOq?usp=sharing (Last time changed at 24/8/2025)

Appendix B: Ten UG Basic Rules for Use of AI in Teaching

Ten UG basic rules for the use of AI in teaching

Please note: additional rules may apply at the level of individual faculties, degree programmes, and course units.

1. AI tools may be used as aids to support general functionalities (study tool/assistant/input for own work). General functionalities include, for example, brainstorming, gaining inspiration, summarizing general information, fine-tuning own work (language correction, language assistant), translation, and independent study/sparring partner (generating mock exam questions and answers). Please note: AI tools are not reliable academic sources and their output must always be processed critically in accordance with academic ways of working. Students are always responsible for their own submitted work.
2. When GenAI functionalities are used (to create new content or replace own work), this should always be mentioned/referred to. The most important difference with the functionalities listed under rule 1 is that GenAI serves to partly replace or outsource one's own working and learning process. If a student uses GenAI in any way other than those described under rule 1, they should explicitly mention this. This also enables the lecturer to give more targeted feedback about acquiring academic ways of working and learning to use tools in a responsible way. Any such use must be mentioned/referred to in a recognizable way, for example under methods/sources/references. The following should at least be stated:
    1. name and version of the tool
    2. for what purpose and how it was used

    Please note: individual degree programmes and course units may set further requirements to the form and content of references, for example a more detailed explanation of the use, examples of prompts entered, reflection on reliability and bias, and verification of information.

3. Any additional rules with regard to the use of GenAI functionalities in addition to the above-mentioned rules 1 and 2 must be communicated before the start of the course unit in question . When in doubt, ask the lecturer. Using tools for functionalities other than those listed under rule 1 may be permitted, partly permitted, or not permitted. This may vary per degree programme and per course unit, because it depends on the

learning outcomes. Students will be notified about this in good time (before the start of the course unit in question), in any case via the syllabus/Brightspace.

4. Using AI tools is regarded as cheating if:
    1. the work submitted cannot sufficiently be considered to be the student's own work, so that their knowledge, understanding, and skills as described in the learning outcomes cannot be assessed and evaluated. Outsourcing work to a tool (or to someone else) to such an extent is not permitted because it affects the heart of academic ways of working. Students must always be able to take responsibility for verifying and analysing information, and for their own academic substantiation. Lecturers teach students to understand this link.

       Or
    2. the student has not correctly mentioned/referred to the use. Submitting a literal copy of GenAI output (or any other output) as own work is never permitted. The definitions of cheating/plagiarism as set out in the Teaching and Examination Regulations of the relevant degree programme apply. The Board of Examiners of the degree programme must determine for each individual case whether it constitutes a case of cheating.
5. Use the positive functionalities of AI tools, but do so consciously and critically. AI tools offer lots of great opportunities. However, using tools also involves risks with regard to the reliability of output (factual errors, biases, non-existing references) and the processing of data (infringement of copyrights and privacy, security, and storage of personal, company, and research data). You should therefore not enter sensitive information or data. Follow the GDPR. Users are personally responsible for using AI tools consciously, critically, and responsibly.
6. Processing agreements/UG licences are a precondition for requiring the use of tools in teaching. If there is no processing agreement between the UG and the owner of the tool, and/or there is no UG licence, students may not be required to create a personal account or to purchase a tool (or a version with more functionalities). In such cases, a similar alternative that is free of charge must be offered. This also applies to open-source tools. Proper processing and storage of personal information and data must be in place if use in teaching is required, and students must have equal tools at their disposal.
7. Scores of AI detection tools do not constitute evidence for cheating. Cheating scores that are generated by AI detection tools may not be used to prove that a student has cheated, because these scores are unreliable (high risk of incorrect scores and lack of transparency about how the tools work). Examiners are responsible for checking the authenticity of submitted work, assessing the work, and reporting any suspicions of cheating/plagiarism to the Board of Examiners of the degree programme in question. Boards of Examiners are responsible for determining whether cheating/plagiarism has indeed been committed and for giving students suspected of cheating/plagiarism the opportunity to put their case.
8. Lecturers bear final responsibility for the assessment of students and the content of the teaching. Lecturers are encouraged to use aids in their teaching and assessment, such as automated marking of multiple-choice exams in accordance with predefined answers. However, automated decision-making/marking based on a GenAI model, without any human checks of the assessment process, is not permitted. The relevant examiner legally bears final responsibility for administering examinations and determining their results.

9. Any adjustments to modes of assessment in order to ensure the validity of assessments must be communicated in good time. The lecturer may conduct an additional oral check when cheating is suspected. In order to ensure the validity of assessment, it may be necessary to adjust a mode of assessment, for example, from a written exam to an oral exam. This is only permitted if the learning outcomes can still be determined. Students must be notified in good time (via Ocasys) and adjustments to modes of assessment during an academic year are in principle not permitted, except in cases of force majeure. In addition, lecturers may conduct additional checks in the form of oral tests when cheating is suspected. These tests do not constitute additional examinations. Students must, however, be notified of this possibility in advance.
10. Interim checks are conducted for theses/final projects. The thesis or final project is an important part of the degree programme, in which many of the learning outcomes are assessed. Interim checks (for example in the form of a meeting or an intermediate product) are therefore conducted to assess the authenticity of the work and the creation process. These checks are often already conducted. Interim checks may count towards the final assessment, although this is not a requirement.

Appendix C: Declaration on the use of generative AI systems during BME projects

Link to signed document: https://acrobat.adobe.com/id/urn:aaid:sc:eu:c2c23c02-74f9-4b9e-ae64-97716aa21cc8